# Structural and Mutational Studies of the Carboxylate Cluster in Iron-Free Ribonucleotide Reductase R2[†]

Martin E. Andersson,[‡,#] Martin Högbom,[‡,§,#] Agnes Rinaldo-Matthis,[‡] Wolfgang Blodig,[‡] Yuhe Liang,[∥] Bert-Ove Persson,[⊥] Britt-Marie Sjöberg,[⊥] Xiao-Dong Su,[∥] and Pär Nordlund*[,‡]

*Department of Biochemistry and Biophysics, Stockholm University, SE-106 91 Stockholm, Sweden, Department of Biochemistry, Life Science College, Peking University, 100871, Beijing, China, and Department of Molecular Biology and Functional Genomics, Stockholm University, SE-106 91 Stockholm, Sweden*

*Received November 21, 2003; Revised Manuscript Received April 8, 2004*

ABSTRACT: The R2 protein of ribonucleotide reductase features a di-iron site deeply buried in the protein interior. The apo form of the R2 protein has an unusual clustering of carboxylate side chains at the empty metal-binding site. In a previous study, it was found that the loss of the four positive charge equivalents of the diferrous site in the apo protein appeared to be compensated for by the protonation of two histidine and two carboxylate side chains. We have studied the consequences of removing and introducing charged residues on the local hydrogen-bonding pattern in the region of the carboxylate cluster of *Corynebacterium ammoniagenes* and *Escherichia coli* protein R2 using site-directed mutagenesis and X-ray crystallography. The structures of the metal-free forms of wild-type *C. ammoniagenes* R2 and the mutant *E. coli* proteins D84N, S114D, E115A, H118A, and E238A have been determined and their hydrogen bonding and protonation states have been structurally assigned as far as possible. Significant alterations to the hydrogen-bonding patterns, protonation states, and hydration is observed for all mutant *E. coli* apo proteins as compared to wild-type apo R2. Further structural variations are revealed by the wild-type apo *C. ammoniagenes* R2 structure. The protonation and hydration effects seen in the carboxylate cluster appear to be due to two major factors: conservation of the overall charge of the site and the requirement of electrostatic shielding of clustered carboxylate residues. Very short hydrogen-bonding distances between some protonated carboxylate pairs are indicative of low-barrier hydrogen bonding.

Enzymes with buried metal centers at their active sites encompass many important proteins, such as methane monooxygenase (MMO)[1], the cytochrome p450s, cytochrome *c* oxidase, and photosystem II (*1*−*3*). The burial of a charged metal center and its ligands in the core of proteins could potentially constitute a major energetic problem by disturbing the formation of the hydrophobic core, which for most proteins is the principal driving force for folding and stability.

Some proteins bind metal ions as complexes with small organic compounds such as protoporphyrin derivatives, i.e., heme, chlorophyll, and B12 (*2*, *3*). In these cases, the charge of the metal is at least partially compensated for by the organic ligand. Extensive hydrophobic interactions can also be made to the hydrophobic moiety of the organic cofactor, further lowering the energetic cost for the burial of the charged metal in the low dielectric core of proteins.

In cases where enzymes bind *free* metal ions to their interior, a more problematic scenario emerges. The interiors of these proteins allow less of a hydrophobic core to form because of the polar/charged nature of the metal and its ligands. Most metalloenzymes appear to be fully folded prior to metal insertion. The metal-binding protein side chains are generally found in very similar positions in both apo and metal-bound forms. However, the charged protein residues needed to stabilize the bound metal are likely to be destabilizing to the metal-free protein when clustered in the protein core. Some residues, such as tyrosinate and cysteinyl ligands, are readily protonated in the apo form, preventing charge build up in the core of the apo protein. Other residues, such as the carboxylate residues glutamate and aspartate, are normally not readily protonated in proteins at neutral pH and considerable energetic costs are associated with their protonation. In water, the carboxylate side chains of glutamate and aspartate have p$K_a$ values in the range of 4−4.5, and although carboxylate residues often play important roles in acid−base catalysis, they are only transiently protonated in these instances (*4*). Buried carboxylate groups have also been implied as major components in proton-transfer pathways through integral-membrane proteins, for example in cytochrome *c* oxidase and bacteriorhodopsin (*5*, *6*). The elucidation of detailed mechanisms of proton transfer in these systems is a major challenge, and for this purpose, a deeper

[†] This work was supported by the Swedish Research Council (VR) and the European Union EU-TMR under contract no. FMRX-CT98-0207.

* To whom correspondence should be addressed. Tel: +46-8-5537 8587. Fax: +46-8-5537 8358. E-mail: par.nordlund@dbb.su.se.

[‡] Department of Biochemistry and Biophysics, Stockholm University.

[§] Present address: Department of Cell and Molecular Biology, Uppsala University, Biomedical Center Box 596, SE-751 24, Uppsala, Sweden.

[∥] Peking University.

[⊥] Department of Molecular Biology and Functional Genomics, Stockholm University.

[#] M.A. and M.H. contributed equally to this work.

[1] Abbreviations: RNR, ribonucleotide reductase; MMO, methane monooxygenase; MES, 2-(*N*-morpholino)ethanesulfonic acid; rms, root mean square.

10.1021/bi036088l CCC: $27.50 
Published on Web 05/22/2004

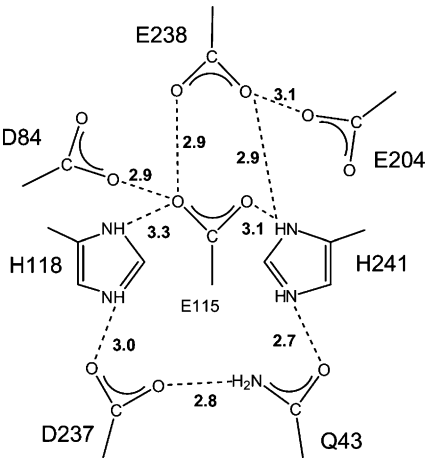


FIGURE 1: Schematic drawing of the detailed geometry of the active site of the wild-type apo *E. coli* R2 di-iron site, adapted from ref *7*. The potential hydrogen bonds are drawn as dashed lines between the hydrogen donor and acceptor atoms, with distances shown in angstroms.

general understanding of the protonation behavior of buried carboxylate residues is desirable.

In ribonucleotide reductase R2 (RNR R2), the formation of the diferric center occurs by binding ferrous ions to a fully folded apo protein, followed by oxidation by molecular oxygen. The three-dimensional structure of apo R2 has previously been determined and is very similar to the native diferrous and diferric forms (*1*, *7*, *8*). The only differences are relatively small changes in the region where the iron atom binds. On the basis of the hydrogen-bonding distances in the wild-type R2 apo structure (Figure 1), it was predicted that the absence of positively charged ferric ions is partially compensated by protonation of two histidines: His118 and His241. In addition, the hydrogen-bonding pattern is suggestive of a minimum of two protonated carboxylates resulting in a loss of two formal negative charges. Therefore, the accumulated change in the net charge upon binding of two ferrous ions to the empty metal site in apo R2 would be zero, and four protons should be released in this process. In bacterioferritin, which has a di-iron center very similar to that of protein R2, the release of four protons for each bimetal-binding site upon metal binding has been directly observed (*9*), which further supports the charge neutrality scenario previously proposed for the metal binding to this family of di-iron proteins (*7*).

The driving force for protonation of the buried side chains, made at a significant energetic cost, is the intrinsically low polarizability of the environment of the di-iron site. This could be understood in terms of the low dielectric constant expected for the interior of a protein. However, in the case of RNR R2, the iron site region is relatively polar and, in principle, the dipolar groups in this region could respond to charge changes by compensatory realignments, minimizing the charge build up so that little or no protonation is required. However, this does not appear to be the case for the wild-type protein.

Charge neutrality scenarios have been implied during the reaction cycle for a number of other metalloproteins, for example, cytochrome *c* oxidase (*10*), photosystem II (*11*), protocatechuate 3,4-dioxygenase (*12*), MMO, and R2 (*8*, *13*). However, an extended understanding of the polarization properties of the local surrounding of the active site of these proteins is still limited.

In the current paper, we have studied the changes in hydrogen-bonding patterns of the metal ligands found in the interior of the R2 protein of ribonucleotide reductase to shed further light on the ability of these protein cores to respond to electrostatic changes.

## MATERIALS AND METHODS

*Protein Preparation.* The plasmid construction and site-directed mutagenesis of the alanine iron ligand mutants have been described previously (*14*). The vector for expressing the S114D mutant was constructed from plasmid pTB2 according to the MUTA-GENE Phagemid in vitro mutagenesis kit (Bio-Rad Laboratories). The primer used in the mutagenesis reaction had the sequence 5′-CTG GGC GTT C**GA C**GA AAC GAT TC-3′. Bold letters indicate the bases that differ from the wild-type sequence. The D84N mutant protein was expressed from a derivative of the pTB2 plasmid generated using the QuickChange mutagenesis kit (Stratagene). The mutagenesis primers had the sequences 5′-CAG ACG CTG CTG **A**AT TCC ATT CAG GGT CGT AGC-3′ and 5′-GCT ACG ACC CTG AAT GGA AT**T** CAG CAG CGT CTG-3′. The resulting mutant plasmids were sequenced in their entirety to verify the correct sequence.

Overproduction and purification of the mutant proteins were done as for wild-type R2 (*15*), with modifications to suit the crystallization experiments. In brief, the protein purification steps include precipitation by streptomycin sulfate and ammonium sulfate; DEAE anion-exchange chromatography; Superose-12 gel filtration or Mono Q ion-exchange chromatography; and finally concentration and exchange of buffers by centrifugal concentration. There was no addition of ferrous ion during cell growth and protein purification.

*Crystallization and Data Collection.* The crystallization of the *Escherichia coli* apo proteins were carried out in Petri dishes by the hanging-drop vapor diffusion method at the same conditions as the wild-type R2 protein (*16*) but with variations in the concentration of the precipitant PEG 4000. The mutant protein crystals are isomorphous to the wild-type crystals, belong to space group $P2_12_12_1$, contain one dimer per asymmetric unit, and have cell dimensions very close to that of the wild-type crystals, $a = 74.3$ Å, $b = 85.5$ Å, and $c = 115.7$ Å. Some crystals were small and fragile, and the completeness of the data is therefore somewhat limited. However, as far as we can judge from the electron density and the refinement behavior, this does not impose a significant limitation on the structural analysis. The apo *Corynebacterium ammoniagenes* protein was crystallized as previously described for the iron-containing protein (*17*). Even though the crystallization conditions were the same, the apo protein crystallized in a different crystal form than the metal-loaded protein. The space group is still $P2_1$ but with cell parameters of $a = 48.9$ Å, $b = 86.5$ Å, and $c = 70.6$ Å, the unique angle $\beta = 105.5°$, and only one dimer per asymmetric unit.

The data for the *E. coli* mutant proteins were collected on rotating anode sources, processed and reduced by online programs on the Hamlin−Xuong detector for E115A, by XDS (*18*) on the Xentronics area detector for H118A and

Table 1: Data Collection and Refinement Statistics

| structure | D84N | S114D | E115A | H118A | E238A | *C. ammoniagenes* |
|---|---|---|---|---|---|---|
| resolution (Å) | 15−2.0 | 20−2.0 | 6.0−2.2 | 6.0−2.2 | 6.0−2.2 | 20−1.63 |
| (outer shell) | (2.10−1.99) | (2.12−2.01) | (2.32−2.20) | (2.32−2.20) | (2.32−2.20) | (1.69−1.63) |
| unique reflections | 42 016 | 38 661 | 30 512 | 32 648 | 28 537 | 63 541 |
| $R_{merge}$[a] | 0.053 | 0.096 | 0.090 | 0.081 | 0.082 | 0.054 |
| completeness (%) | 88 | 80 | 83 | 91 | 81 | 95 |
| (outer shell) | (82) | (91) | (60) | (78) | (68) | (87) |
| $I/\sigma(I)$ | 20.1 | 12.9 | 10.5 | 9.7 | 6.1 | 17.1 |
| (outer shell) | (6.6) | (5.3) | (6.9) | (3.9) | (2.8) | (3.9) |
| $R$ factor | 0.213 | 0.202 | 0.199 | 0.186 | 0.187 | 0.165 |
| $R_{free}$ | 0.256 | 0.244 | 0.246 | 0.239 | 0.251 | 0.222 |
| RMS[b] of bonds | 0.006 | 0.006 | 0.006 | 0.006 | 0.008 | 0.018 |
| RMS[b] of angles | 1.09 | 1.02 | 1.18 | 1.08 | 1.32 | 1.75 |
| average B main chain (Å$^2$) | 38.5 | 30.3 | 22.7 | 26.5 | 24.9 | 20.0 |
| average B side chain (Å$^2$) | 41.6 | 37.5 | 23.4 | 28.9 | 26.4 | 26.0 |
| water molecules | 236 | 310 | 232 | 196 | 216 | 898 |

[a] $R_{merge} = \Sigma|I_{obs} - I_{avg}|/\Sigma I_{obs}$, where the summation is over all reflections in the data set. [b] RMS of bonds and angles are the root-mean-square deviations from ideal values of the bond lengths and angles in the final structures.

E238A and by Denzo and Scalepack (*19*) for D84N and S114D. For the apo *C. ammoniagenes* crystals, data was collected on a MAR detector at the Max Laboratory synchrotron in Lund and processed by Denzo and Scalepack (*19*). Further processing and evaluation of the data sets was done with the CCP4 program suite (*20*) (Daresbury Lab., U.K.). Data sets were collected on nonfrozen crystals except for the *E. coli* D84N and the *C. ammoniagenes* apo protein. The data were cut so that the $R_{merge}$ in the highest resolution shell was between 20 and 30% for all datasets. Data collection statistics are shown in Table 1.

*Structure Determination.* The structure determination of the five *E. coli* mutant proteins was started by CNS refinement (*21*) using the diferrous R2 structure (*8*) as a starting model. For the *E. coli* metal ligand mutants, structures were determined from the apo form of the protein. In the D84N mutant structure, one di-iron site still contained some iron density and was excluded from a detailed analysis. The *E. coli* S114D mutant was determined in its diferric state. After the initial refinements, the $R$ factors were down to approximately 25%. The $2F_o - F_c$ and $F_o - F_c$ maps were examined, and the structures were adjusted with Quanta (Molecular Simulations Inc.) wherever necessary. Water molecules were introduced in the process but excluded when $B$ factors exceeded 60.0 Å$^2$. The structure of the *C. ammoniagenes* apo protein was solved by molecular replacement using the CNS software package (*21*) with the refined structure of the *C. ammoniagenes* R2F (*17*) as the search model. Once the correct solution was found, only minor manual rebuilding alterations combined with simulated annealing refinement and introduction of water molecules were necessary to produce the final model. The *C. ammoniagenes* protein structure displays some residual density at the iron positions. The high resolution of the data allowed us to refine their occupancy and estimate the amount of iron present, which in all cases converged to an occupancy below 25%. The contribution from iron-containing sites is thus unlikely to influence the observed ligand conformations significantly. The Fe atoms with low occupancy were kept in the model during subsequent refinement and analysis to minimize disturbance of the electron density for the metal ligands. The statistics of the final refinement are shown in Table 1.

## RESULTS

The overall fold of the structures of the apo *C. ammoniagenes* R2 as well as the mutant *E. coli* proteins D84N, S114D, E115A, H118A, and E238A are very similar to that of the corresponding iron-containing wild-type R2 protein. The structures show that neither introduction or removal of a buried, potentially charged, side chain, nor the substitution of a metal ligand has any major effect on the folding of the R2 proteins. In fact, the Cα rms deviations, which are between 0.25 and 0.29 Å for the apo mutants compared with wild-type apo and diferrous R2, are smaller than the differences between the two noncrystallographically related subunits of the dimeric protein in the same crystal (the mutants as well as the wild type), which are typically 0.5−0.6 Å.

The detailed geometry for each structure with distances between possible hydrogen-bonding pairs is shown in Figure 2. In all of the structures, there is at least one short distance indicative of a hydrogen bond between two carboxylate groups. The crystal structures of E115A and E238A reveal one potential carboxylate−carboxylate hydrogen bond in each case (parts a and b of Figure 2), the Glu238/Glu204 pair in the E115A protein and the Glu115/Asp84 pair in the E238A mutant. Although additional protonation of carboxylates in these mutants cannot be excluded; on the basis of the current paper, it appears less likely. The hydrogen-bonding pattern is also consistent with positively charged histidines H118 and H241. Hence, the net charge change of the ligand spheres of the apo forms of E115A and E238A, as compared to the wild-type protein, is most likely zero.

The deletion of the histidine side chain in the H118A mutant protein constitutes a removal of one potential positive charge from the buried metal site. The hydrogen-bonding pattern of the carboxylate ligands is similar to *E. coli* apo wild-type R2 but with one additional short carboxylate−carboxylate distance, suggesting three protonated carboxylate ligands (Figure 2c). In this case, additional protonation appears unlikely and the net change of charge is most likely zero for the ligand sphere as compared to the wild-type apo protein.

In the D84N protein, the distance is short between the two carboxylate pairs, E238/E115 and E238/E204, suggesting the protonation of two carboxylate residues (Figure 2d). At the

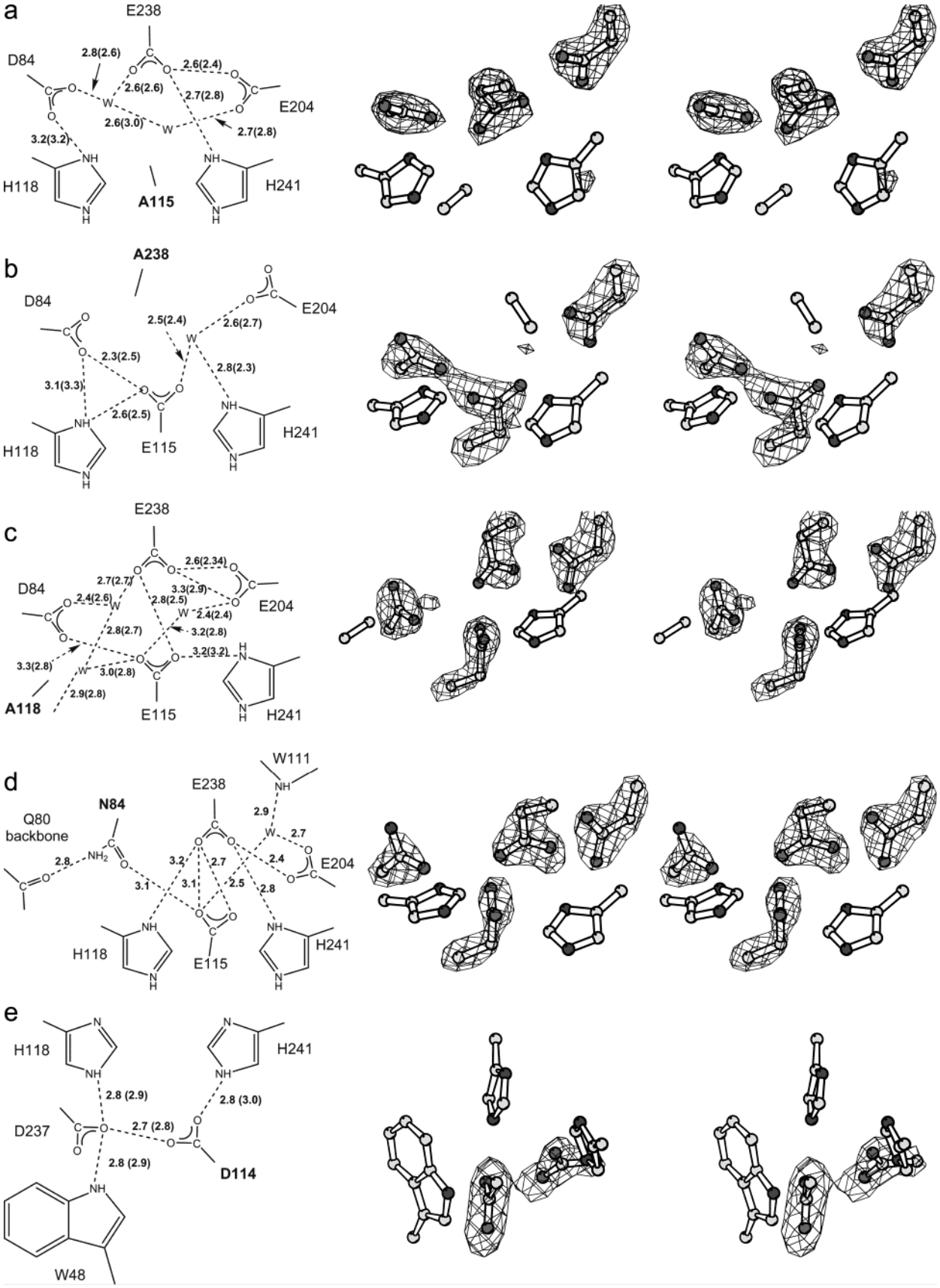


FIGURE 2: Schematic drawing of the detailed geometry of the active site of the five *E. coli* mutant proteins. Electron density is a stereoview of a simulated annealing $F_o - F_c$ map with the carboxylate side chains omitted from the map calculation, (a) E115A, (b) E238A, (c) H118A, (d) D84N, and (e) S114D. The potential hydrogen bonds are drawn as dashed lines between the hydrogen donor and acceptor atoms, with distances shown in angstroms. In the cases where two distances are given, they refer to the distances for each of the two noncrystallographically related subunits of the R2 dimer. The mutated residues are indicated with bold letters.

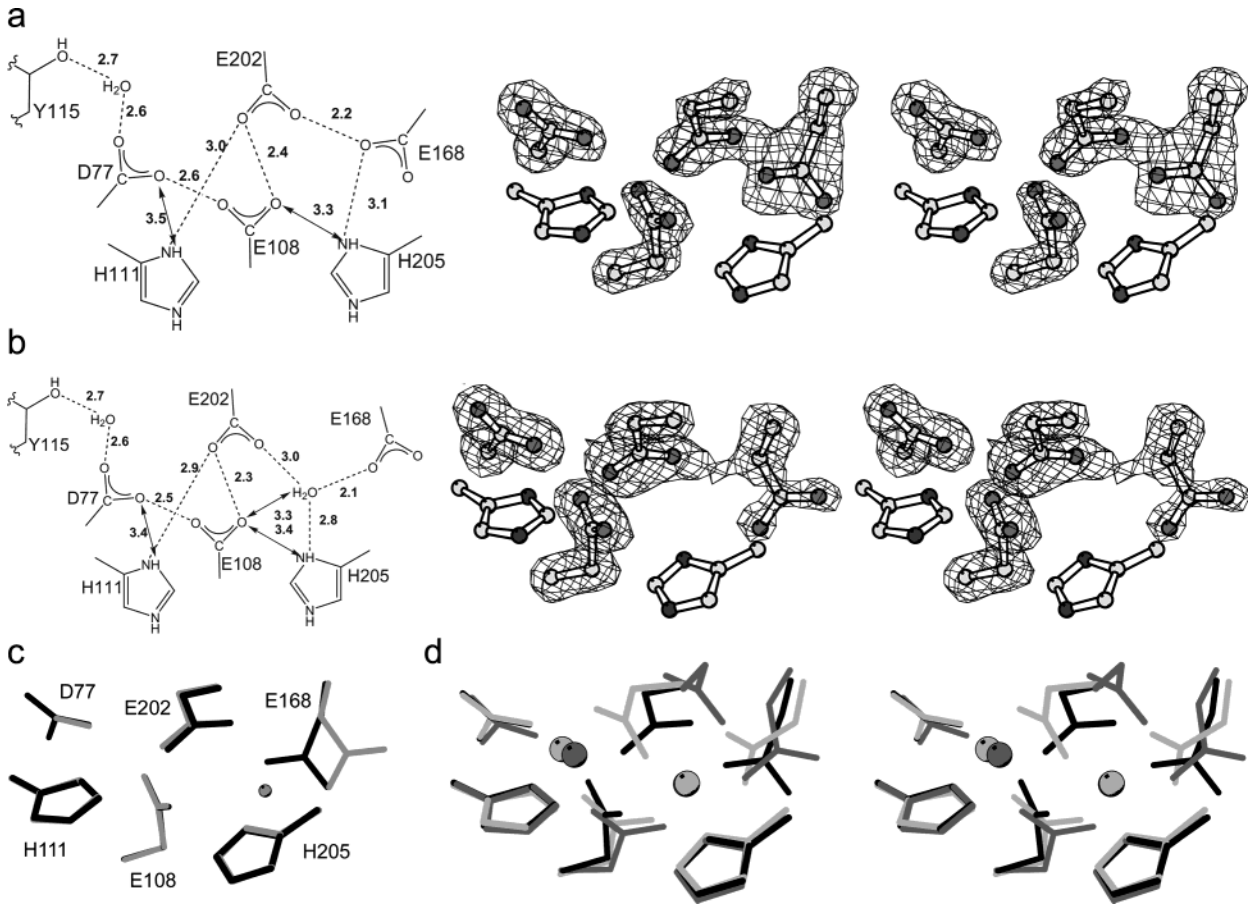


FIGURE 3: Schematic drawing of the detailed geometry of the active site of the wild-type apo *C. ammoniagenes* R2 sites. Electron density is a stereoview of a simulated annealing $F_o - F_c$ map with the carboxylate side chains omitted from the map calculation, (a) site A and (b) site B. The potential hydrogen bonds are drawn as dashed lines between the hydrogen donor and acceptor atoms, with distances shown in angstroms. (c) Comparison of site A (black) and site B (gray). (d) Stereoview of a superposition of the *C. ammoniagenes* apo site A (black), the reduced iron-containing site (light gray), and the oxidized iron-containing site (gray).

present resolution, the hydrogen-bonding distances of the histidines are not conclusively determined but strongly supportive of two fully protonated histidines and a net charge of the site of +1.

Serine 114 is found in the second coordination sphere of the iron site and makes a hydrogen bond to H241. The corresponding residue is an aspartate in several other di-iron proteins. This residue hydrogen-bonds to the histidine and also to an arginine found on the surface of the protein. Although S114 is found close to the surface, which could increase the polarizability of this area and potentially allow for the introduction of an extra charge, no obvious net charge change is observed in this mutant when a carboxylate−carboxylate hydrogen bond is made between D114 and D237 (Figure 2e).

The apo *C. ammoniagenes* structure reveals slightly different carboxylate cluster structures in the two crystallographically independent subunits (parts a, b, and c of Figure 3). Glutamate 168, corresponding to E204 in *E. coli* R2, has two different conformations in the two subunits. The conformation of E168 in the B subunit allows a water molecule to bind to the site. The difference observed in the two subunits is most likely due to the different environment of the monomers in the crystal lattice, introducing long-range conformational effects on the carboxylate cluster. However, the structural origin of these effects is not obvious based on the present structure. The difference in the solvation of the site also results in different protonation patterns in the two different subunits. Subunit A (Figure 3a) appears to form three protonated carboxylate pairs, while two pairs are formed in subunit B (Figure 3b) based on the intercarboxylate distances. The net charge distribution in these sites is, however, unclear when the assignment of the protonation states of His 205, on the basis of distances, is ambiguous.

The two sites in the *C. ammoniagenes* apo structure are very similar to each other apart from the rotamer change of E168 (Figure 3c). When the reduced (light gray in Figure 3d) and oxidized (gray in Figure 3d) iron-containing sites are compared, three of the carboxylates change conformation to produce the tightly hydrogen-bonded apo site (site A in black).

Aside from the changes in the protonation and hydration patterns in the metal site, only very minor local changes of the surrounding of the sites are seen and no significant changes extending further than 8 Å from the site are observed in any of the structures. The observed local changes are all small translational movements of atoms, and no obvious case is found where polar groups appears to have changed their orientation.

## DISCUSSION

The four iron−ligand mutant proteins (D84N, E115A, H118A, and E238A) of this paper have all been purified as

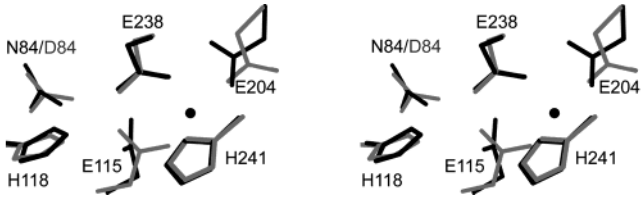


FIGURE 4: Stereo drawing of the comparison of the apo D84N structure (black) and the apo wild-type structure (gray). Note how this mutation introduces conformational changes throughout the metal-binding site and leads to the introduction of a water molecule into the active site.

apo proteins, suggesting that they have significantly lower affinity for iron than the wild-type protein. Earlier studies have shown that three of the mutants, E115A, H118A, and E238A, can bind ferrous ion in solution, and in the case of H118A, a tyrosyl radical is also generated (*14*). Soaking the experiment of E238A crystals with ferrous ions showed that E238A incorporated metal ions in the metal-binding site and was capable of activating $O_2$ to yield hydroxylation of the nearby F208 residue (*22*), while on the other hand, E115A crystals did not bind significant amounts of iron even after more than 10 h of soaking in 20 mM $FeCl_2$ (Su, X. D., unpublished). The D84N protein binds iron and generates a tyrosyl radical, although in a very slow reaction (Blodig, W., unpublished).

In each of the alanine mutant structures of *E. coli* R2, water molecules occupy the cavity created by the mutation. In E115A, two well-defined water molecules are located close to the position of the Glu115 side chain in wild-type apo R2 (Figure 2a). In the E238A mutant, one well-defined water molecule is found bound in the ligand sphere (Figure 2b). In H118A, three new water molecules are found at the carboxylate cluster (Figure 2c). Interestingly, in the D84N mutant, in which the asparagine side chain would be expected to occupy a similar volume as the aspartate side chain, one additional water molecule is still found in the carboxylate cluster (Figure 2d and Figure 4). In these structures, most water molecules appear to bridge two carboxylate groups by donating hydrogen bonds to both of them, thereby serving as an electrostatic and steric shield between the repelling charges of the carboxylates.

The *C. ammoniagenes* and *E. coli* structures presented show short hydrogen bond distances between carboxylate groups. These hydrogen bonds are 0.3−0.4 Å shorter than the 2.7 Å expected as a lower limit for −O−H···O− hydrogen bonds (*23*). The higher resolution (1.63 Å) and the good *R* factor (16.5%) of the *C. ammoniagenes* R2 structure make this observation unambiguous. The accuracy of the hydrogen-bond distances deduced from the crystal structures of the *E. coli* proteins determined at 2.0−2.2 Å resolution is however more limited. Unfortunately, no appropriate methods exist for coordinate error estimates for individual atoms in protein crystal structures at similar resolutions. Typically, the Luzzati plot derived global errors at this resolution are in the order of 0.2 Å, and residues in the core of the protein are expected to be significantly better defined than the surface residues. Thus, the few cases where large distance differences (g.t. = 0.3 Å) are seen between the two noncrystallographically related subunits are probably rather due to the distortions present between the two subunits, caused by crystal packing and the slightly different solvation, than a direct measure of the accuracy of the structure. The repeated observation of short carboxylate−carboxylate hydrogen-bonding distances in the apo R2 proteins supports the observation that these carboxylate−carboxylate hydrogen bonds are shorter than the "expected" 2.7 Å. Therefore, we conclude that the carboxylate−carboxylate pairs of R2 proteins, in some cases, form unusually short interactions indicative of so-called "low barrier" hydrogen bonds (*24*). These types of hydrogen bonds are usually found where the p$K_a$ value of the hydrogen-bond donor and acceptor are very similar and the proton can be considered to be shared equally by the two groups.

Except in the case of D84N, the structures of the R2 carboxylate cluster support a net charge change of zero upon metal binding, although this observation has not been unambiguously proven at the limited resolution of the structural studies. From these and previous R2 studies, it appears that the protein regions surrounding the di-iron site are indeed poor at stabilizing charge build up. The alanine mutants also add some space for structural optimization by allowing the appropriate protonation and hydrogen bonds to be formed for stabilizing the charge neutral structures. In the D84N mutant, however, the acceptance of a net charge accumulation could be explained by steric crowding of the cluster region combined with shielding of the carboxylate interactions from each other by protonation and introduction of a water molecule. An alternative explanation could be that one of the His ligands is not fully protonated, which would give a charge neutral center.

The structural and mutagenesis data of the present paper do allow tentative protonation states to be assigned but do not give direct information on p$K_a$ values when all experiments have been done at a constant pH (pH 6.0 for *E. coli* and 6.5 for *C. ammoniagenes*). In fact, it might be that protonation is needed to stabilize the fully folded protein, and therefore, p$K_a$ values, if measured, would include a major structural transition and not only a local protonation event. However, in some long-range proton transfer systems, buried carboxylate residues have been implicated as major participants, with only small local structural changes. Bacteriorhodopsin is one of the best characterized proton-transfer systems and has four buried carboxylate residues in the channel, where protons are expected to exit from the photoactivated retinal (*6*). One pair of carboxylates, Asp85 and Asp212, is located close to the retinal, and Asp85 is suggested to be the primary proton acceptor in the reaction. E194 and E204 are found closer to the cytoplasmic surface and play a role in proton release. An FTIR study suggests a delocalized proton site could potentially be an important feature for promoting proton transfer in bacteriorhodopsin (*25*). The observed protonation of carboxylate pairs in the R2 carboxylate cluster support the notion that the protonation of carboxylate pairs can lead to resonance-type structures, where protons are shared between the two carboxylate groups.

In conclusion, the current paper shows that the hydrogen-bonding pattern in the carboxylate cluster of R2 can change quite dramatically upon mutation and that the hydration and protonation state of the carboxylate cluster can be modulated to obtain energetically acceptable interactions without distorting the overall fold of the protein. These observations appear to be due to two effects: the neutralization of charge

build up at the site, which is most striking for the H118A mutant, and the "shielding" of potential unfavorable carboxylate interactions caused by steric clustering at the site. The shielding is achieved either by formation of a carboxylate−carboxylate hydrogen bond or by the introduction of an intervening water molecule. The present data therefore suggest that, in systems where the carboxylate residues have some flexibility, a preference for zero charge exists, while in sterically restrained systems, such as the D84N mutation, net charge build up might be observed even in a low dielectric environment. These observations may have some bearing on the potential for charge build up in reaction intermediates of the protein R2 catalyzed reactions. The presence of water molecules at the iron site in all four of the iron ligand mutants studied in the current paper is in contrast to what was found in the wild-type apo R2, which has no such water molecules. This supports the notion that the compact clustering of carboxylate side chains, as seen in the wild-type R2, is important for both the efficiency and specificity of iron binding. A binding scenario is possible where two neutral ferrous-hydro-hydroxy$_2$ clusters penetrate the protein to bind the site and where the protons from the carboxylates are accepted by the leaving hydroxides.

## ACKNOWLEDGMENT

We would like to extend thoughts of gratitude to the late Markku Saarinen for help with data collection on the Hamlin−Xuong detector. We are grateful to Yngve Cerenius and Anders Svensson for assistance with data collection and the Max Laboratory in Lund for providing synchrotron time.

## REFERENCES

1. Nordlund, P., Sjöberg, B.-M., and Eklund, H. (1990) Three-dimensional structure of the free radical protein of ribonucleotide reductase, *Nature 345*, 593−598.
2. Lippard, S. J., and Berg, J. M. (1994) *Principles of Bioinorganic Chemistry*, University Science Books, Sausalito, CA.
3. Williams, R. J. P., and Silvia, J. J. R. F. d. (1996) *The Natural Selection of the Chemical Elements: The Environment and Life's Chemistry*, Clarendon Press, Oxford, U.K.
4. Fersht, A. (1985) *Enzyme Structure and Mechanism*, W. H. Freeman and Company, New York.
5. Iwata, S., Ostermeier, C., Ludwig, B., and Michel, H. (1995) Structure at 2.8 Å Resolution of Cytochrome *c* Oxidase from *Paracoccus denitrificans*, *Nature 376*, 660−669.
6. Heberle, J. (2000) Proton-transfer reactions across bacteriorhodopsin and along the membrane, *Biochim. Biophys. Acta Bioenerg. 1458*, 135−147.
7. Åberg, A., Nordlund, P., and Eklund, H. (1993) Unusual clustering of carboxyl side-chains in the core of iron-free ribonucleotide reductase, *Nature 361*, 276−278.
8. Logan, D. T., Su, X. D., Åberg, A., Regnström, K., Hajdu, J., Eklund, H., and Nordlund, P. (1996) Crystal structure of reduced protein R2 of ribonucleotide reductase: The structural basis for oxygen activation at a dinuclear iron site, *Structure 4*, 1053−1064.
9. Keech, A. M., Le Brun, N. E., Wilson, M. T., Andrews, S. C., Moore, G. R., and Thomson, A. J. (1997) Spectroscopic studies of cobalt(II) binding to *Escherichia coli* bacterioferritin, *J. Biol. Chem. 272*, 422−429.
10. Michel, H. (1999) Cytochrome *c* oxidase: Catalytic cycle and mechanisms of proton pumping—A discussion, *Biochemistry 38*, 15129−15140.
11. Hoganson, C. W., and Babcock, G. T. (1997) A metalloradical mechanism for the generation of oxygen from water in photosynthesis, *Science 277*, 1953−1956.
12. Frazee, R. W., Orville, A. M., Dolbeare, K. B., Yu, H., Ohlendorf, D. H., and Lipscomb, J. D. (1998) The axial tyrosinate $Fe^{3+}$ ligand in protocatechuate 3,4-dioxygenase influences substrate binding and product release: Evidence for new reaction cycle intermediates, *Biochemistry 37*, 2131−2144.
13. Andersson, M. E., Högbom, M., Rinaldo-Matthis, A., Andersson, K. K., Sjöberg, B. M., and Nordlund, P. (1999) The crystal structure of an azide complex of the diferrous R2 subunit of ribonucleotide reductase displays a novel carboxylate shift with important mechanistic implications for diiron-catalyzed oxygen activation, *J. Am. Chem. Soc. 121*, 2346−2352.
14. Persson, B. O., Karlsson, M., Climent, I., Ling, J. S., Loehr, J. S., Sahlin, M., and Sjöberg, B. M. (1996) Iron ligand mutants in protein R2 of *Escherichia coli* ribonucleotide reductase—Retention of diiron site, tyrosyl radical, and enzymatic activity in mutant proteins lacking an iron-binding side chain, *J. Biol. Inorg. Chem. 1*, 247−256.
15. Sjöberg, B.-M., Hahne, S., Karlsson, M., Jörnvall, H., Göransson, M., and Uhlin, B. E. (1986) Overproduction and purification of the B2 subunit of ribonucleotide reductase from *Escherichia coli*, *J. Biol. Chem. 261*, 5658−5662.
16. Nordlund, P., Uhlin, U., Westergren, C., Joelsen, T., Sjöberg, B. M., and Eklund, H. (1989) New crystal forms of the small subunit of ribonucleotide reductase from *Escherichia coli*, *FEBS Lett. 258*, 251−254.
17. Högbom, M., Huque, Y., Sjöberg, B. M., and Nordlund, P. (2002) Crystal structure of the di-iron/radical protein of ribonucleotide reductase from *Corynebacterium ammoniagenes*, *Biochemistry 41*, 1381−1389.
18. Kabsch, W. (1988) *J. Appl. Crystallogr. 21*, 916−924.
19. Otwinowski, Z. (1993) pp 56−62, SERC Daresbury Laboratory, Warrington, U.K.
20. Collaborative computational project (1994) *Acta Crystallogr., Sect. C 50*, 760−763.
21. Brünger, A. T., Adams, P. D., Clore, G. M., DeLano, W. L., Gros, P., Grosse-Kunstleve, R. W., Jiang, J.-S., Kuszewski, J., Nilges, M., Pannu, N. S., Read, R. J., Rice, L. M., Simonson, T., and Warren, G. L. (1998) Crystallography & NMR System: A New Software Suite for Macromolecular Structure Determination, *Acta Crystallogr., Sect. D 54*, 905−921.
22. Logan, D. T., deMaré, F., Persson, B. O., Slaby, A., Sjöberg, B. M., and Nordlund, P. (1998) Crystal structures of two self-hydroxylating ribonucleotide reductase protein R2 mutants: Structural basis for the oxygen-insertion step of hydroxylation reactions catalyzed by diiron proteins, *Biochemistry 37*, 10798−10807.
23. Creighton, T. (1993) *Proteins*, W. H. Freeman and Company, New York.
24. Perrin, C. L., and Nielson, J. B. (1997) "Strong" hydrogen bonds in chemistry and biology, *Annu. Rev. Phys. Chem. 48*, 511−544.
25. Rammelsberg, R., Huhn, G., Lubben, M., and Gerwert, K. (1998) Bacteriorhodopsin's intramolecular proton-release pathway consists of a hydrogen-bonded network, *Biochemistry 37*, 5001−5009.

BI036088L